Cancer Nanotechnology

RESEARCH Open Access

Preparation and characterization of the myricetin-loaded solid lipid nanoparticles decorated with folic acid-bound chitosan and evaluation of its antitumor and anti-angiogenic activities in vitro and in vivo in mice bearing tumor models

Niloufar Khatamian[1], Alireza Motavalizadehkakhky[2,3*], Masoud Homayouni Tabrizi[4], Jamshid Mehrzad[1,3] and Rahele Zhiani[2]

*Correspondence: amotavalizadeh@yahoo.com

[1] Department of Biochemistry, Neyshabur Branch, Islamic Azad University, Neyshabur, Iran
[2] Department of Chemistry, Neyshabur Branch, Islamic Azad University, Neyshabur, Iran
[3] Advanced Research Center for Chemistry, Biochemistry and Nanomaterial; Neyshabur Branch, Islamic Azad University, Neyshabur, Iran
[4] Department of Biology, Mashhad Branch, Islamic Azad University, Mashhad, Iran

Abstract

Myricetin is a flavonoid with anticancer properties. This study aimed to formulate myricetin in the form of solid lipid nanoparticles (SLN), decorated with chitosan (CS) and active-targeted with folic acid (FA). After characterization, the in vitro release, cytotoxicity, antioxidant, and ability of the formulation to induce apoptosis using flow cytometry, fluorescent microscopy, and real-time qPCR were examined. Then in vivo anti-angiogenesis on chick chorioallantoic membrane (CAM) and antitumor activities on mice bearing tumor models were investigated. The present study showed that the size of 310 nm and zeta potential of + 30 mV were acceptable for oral administration. The Michaelis–Menten model fitted the drug release pattern with lag during 144 h of the study. The cytotoxicity assay showed that myricetin-SLN-CS-FA significantly killed cancer cells at the concentrations of 6.25, 12.5, 25, 50 and 100 µg/mL (*$p < 0.05$, **$p < 0.01$, and ***$p < 0.001$). The highest level of apoptosis was shown at the concentration of 45 µg/ml in flow cytometry, and fluorescent studies. These results showed the anticancer properties of myricetin-SLN-CS-FA in a dose-dependent manner. The real-time results also indicated that the formulation exerted its cytotoxic effect by activating apoptosis genes. The DPPH, ABTS, and FRAP studies also demonstrated the significant antioxidant properties of the myricetin-SLN-CS-FA (*$p < 0.05$, **$p < 0.01$, and ***$p < 0.001$). The anti-angiogenic activities of the formulations depicted in the CAM assay significantly decrease the number and length of the vessels (*$p < 0.05$, **$p < 0.01$, and ***$p < 0.001$), and also affect VEGF and VEGFR, genes involved in angiogenesis (**$p < 0.01$, and ***$p < 0.001$). The antitumor studies indicated the statistically significant effects of myricetin-SLN-CS-FA on reducing tumor volume (*$p < 0.05$ and ***$p < 0.001$). The H&E staining of the liver and monitoring of the animal weights also indicated the safety of the formulation. The analysis of mRNA expression in liver and tumor

demonstrated that myricetin-SLN-CS-FA exerts its antitumor activities by modulating the inflammatory and oxidative responses in the tissues.

Keywords: Solid lipid nanoparticle, Breast cancer, Myricetin

Introduction

Cancer therapy is an application of one or combination of chemotherapy, radiotherapy, and surgery, most commonly used to treat the disease. Several factors limit the efficacy and selectivity of conventional chemotherapies, including high drug resistance, a lack of tissue tolerance to the drugs, and poor effectiveness (Zhu et al. 2017). To increase the bioavailability of anticancer agents, several nano-drug delivery systems have been investigated over the last few decades. There are several ways in which nanoparticles may be used in the fields of biology, medicine, electrical engineering, and chemistry. Nanoparticles are primarily determined by their size and shape, which are the main determinants of their performance (6). Solid lipid nanoparticles (SLNs) and polymer nanoparticles are potential drug delivery systems (Rahmati et al. 2022; Nasirizadeh and Malaekeh-Nikouei 2020). There are several advantages of SLNs, such as increased ability to load medicine, increased blood circulation period, and regulation of release kinetics, as well as an enhanced ability to treat cancer with anticancer medicines. Furthermore, the embedded compound is protected from chemical degradation by the lipids of the SLNs (Wang et al. 2018; Stella et al. 2018).

SLN residence time could be increased by mucoadhesive interaction in the tumor microenvironment (TME) to further improve the stability of these colloidal systems: mucoadhesion would result in a further decrease in nanoparticle removal from the TME and a simultaneous increase in internalization in tumor cells (Sandri et al. 2010). A cationic polysaccharide, chitosan (CS), has excellent mucoadhesive characteristics, enhances penetration across various tumor types, and inhibits enzyme activity against various proteolytic enzymes (Hamedinasab et al. 2020).

In cancer treatment, tumor-targeted drug delivery systems are emerging as a promising strategy due to their ability to the efficient delivery of their content to the site of action and avoid most of the harmful side effects typically associated with conventional chemotherapy (Mashreghi et al. 2018). The delivery of cytotoxic cargo to cancerous tissue is enabled by targeting specific biomarkers overexpressed on tumor cells, thereby reducing harmful side effects and increasing therapeutic effects (Valeur et al. 2017). In recent years, there has been great interest in the folate receptor (FR). The elevated expression of FR on various cancer cell types makes FR a promising candidate for delivering a compound to tumors via tumor-targeted delivery through its ligand folic acid (FA) (Fernández et al. 2018).

The flavonoids in plants are non-toxic molecules with a variety of biological actions. Flavonoids, including myricetin (3,5,7,3′,4′,5′-hexahydroxyflavone) are present in many edible plants, including berries, oranges, grapes, and herbs (Feng et al. 2015). Recent studies have shown that myricetin is an antitumor in several cancers (Shiomi et al. 2013). Apoptosis resistance and cell cycle arrest result from the activation of oncogenes and/or the inactivation of tumor suppressor genes that cause uncontrolled growth, invasion, and migration of cancer cells (Sarkar et al. 2013). Apoptosis-promoting and cell cycle pathways are mainly inactivated by inactivating apoptosis-promoting genes. Thus,

myricetin is a known apoptotic promoter through its ability to regulate signaling pathways, induce ROS-mediated stress, and damage DNA via endoplasmic reticulum stress (Semwal et al. 2016). Aside from regulating inflammation, myricetin induces protective autophagy, arrests the cell cycle, inhibits invasion, and inhibits migration (Zhang et al. 2018a; Cao et al. 2018).

The aim of this study was to prepare myricetin-loaded SLN (myricetin-SLN). Then modification of the SLN surface using CS and confer its targeted abilities by adding FA (myricetin-SLN-CS-FA) on the surface of the nanoparticle. After characterization of the SLN-CS-FA, the in vitro and in vivo anticancer effects of formulation were evaluated.

Materials and methods

Materials

Myricetin, stearic acid, lecithin, folic acid, NHS, EDC, chitosan (low molecular weight), Tween 80, ABTS, DPPH, and ferric tripyridyl triazine (Fe^{3+} TPTZ), 4′, 6-diamidino-2-phenylindole (DAPI), propidium iodide (PI), acridine orange (AO), and MTT were purchased from Sigma Aldrich (Darmstadt Germany). Human breast carcinoma MCF-7 and human foreskin fibroblast HFF cell lines were obtained from Ferdowsi University of Mashhad cell bank, Iran. All materials and reagents needed for cell culture were provided by Gibco (USA).

Myricetin-loaded SLN nanoparticle preparation

A high-pressure homogenization followed by ultrasound was used to prepare SLN-NPs containing myricetin. In preparation of nanoparticles, myricetin, stearic acid (30 mg), and lecithin (60 mg) were combined with an aqueous phase composed of water (10 ml) and Tween 80 (2% w/v). Next, 10 mg of the myricetin was dissolved in 1 ml of DCM and added to the solution containing stearic acid–lecithin, and immediately the aqueous phase was added to the organic phase and the resulting solution was homogenized. With the help of a high-speed centrifuge, the nanostructures were separated from the surrounding liquid after 24 h of incubation. The amount of drug encapsulation was assessed in the supernatant liquid using HPLC.

Surface decoration of myricetin-loaded SLN with FA-CS

Following the loading of myricetin on SLN-NPs, FA-bound CS was attached to the surface of nanoparticles via EDC and NHS. First, EDC:NHS (1:2 molar ratio) was added to the solution of FA (1% in DMSO) as the starting material. Then acetic acid 1% and CS (8 mg) were added to the mixture, followed by incubation for 24 h. After adjusting the pH of the solution to 9, the FA-CS precipitate was formed. After dialysis, the precipitate was lyophilized in order to remove the free FA. As a next step, the CS-FA precipitate was dissolved in 1% acetic acid and then added to the myricetin-SLN solution dissolved in distilled water. After two hours, the reaction was centrifuged and lyophilized. To measure FA binding, the supernatant was collected.

Characterization of myricetin-SLN-CS-FA

The dynamic light scattering (DLS) method was used to assess the size, distribution, and zeta potential of myricetin-SLN-CS-FA. As part of the measurement, nanoparticle

suspensions were prepared in colloidal suspensions, and then dilution and dispersion of nanoparticles in solvents were measured three times with a Malvern Zetasizer. Scanning electron microscopy (SEM) imaging of the myricetin-SLN-CS-FA was performed to determine their size and morphology. A drop of myricetin-SLN-CS-FA was placed on a grid and allowed to dry at room temperature. Images were taken after nanoparticles were dried and coated with gold. In order to ensure drug loading and surface modification of nanoparticles, the HPLC and FTIR methods were used, respectively. In order to perform a spectroscopic analysis of nanoparticles, compressed tablets containing nanoparticles and KBR were prepared and analyzed using FTIR.

Release study

A dialysis method and an absorption spectrophotometer were used to investigate the release profile of free myricetin and myricetin from nanoparticles. For this purpose, one milliliter of myricetin-SLN-CS-FA was poured into the dialysis bag (12,000–14,000 molecular weight cut-off), and the bag was soaked into phosphate buffer saline (PBS) with pH 7.4 and stirred at 37 °C and 100 rpm. For free myricetin, 1 ml of free myricetin (2 mg/ml in PBS pH 7.4) was poured in dialysis bag and the bag soaked into PBS as mentioned above. After a specified period of time, 1 ml of the solution was removed for analysis, and 1 ml of fresh PBS was added. A release curve was drawn by calculating the release rate and using the myricetin standard absorption chart to determine the myricetin release rate. The prediction of the release model was performed using free, open-source software KinetDS® based on the calculation of the coefficient of determination (R2) (Hamedinasab et al. 2020).

Cytotoxicity assay

The cytotoxicity effect of free myricetin and myricetin-SLN-CS-FA was evaluated against human breast cancer MCF-7 and human foreskin fibroblast HFF cells using the MTT assay. The cells were seeded into 96-well plates (5000 cells\well), and after 24 h, they were treated to serial concentrations of free myricetin and myricetin-SLN-CS-FA. For free myricetin after 48 h and for myricetin-SLN-CS-FA after 24, 48 and 72 h, the treatment medium was removed, and 100 µL of MTT solution was added to each well. After 240 min of incubation, the formazan crystals were dissolved in DMSO, and adsorption of the samples at 570 nm was evaluated (Stat fax 2100). The cell viability was calculated using the following formula (Soltani et al. 2015):

$$\text{Cell viability (\%)} = (\text{OD treated cells} / \text{OD un - treated cells}) \times 100.$$

Anti-apoptotic activities

For analyzing the cell cycle, MCF-7 cells were treated with different concentrations of Myricetin-SLN-CS-FA for 48 h, and after that, the treatment medium was drained. The cells were separated from the plate bottom by using trypsin EDTA to separate them from the plate bottom. After the suspension of cells had been transferred to the microtube, it was centrifuged to separate the cells. Following the washing process, the supernatant was removed from the samples, and 400 µL of PI dye was added to the cell sediment;

10 min later, the cells were analyzed by a flow cytometer (FACSCalibur, Becton Dickinson, USA) (Alhajamee et al. 2021).

To stain the MCF-7 cells with fluorescent dyes, they were cultured in 6-well plates and treated with MTT assay concentrations after 24 h. After 48 h, the treatment medium was drained, and 1 ml of the dye was added to each well. Images were taken under a fluorescent microscope after 48 h. 2 µl of AO and PI (3 mg/ml) were added to 1 ml of PBS to prepare AO/PI dye solution. DAPI dye solution was prepared by adding 1 µL of DAPI dye (1 mg/ml) to 1 ml of PBS.

Real-time qPCR

In order to assess the expression of apoptosis-related genes (Cas3, Cas9, Bax, and Bcl-2), real-time qPCR was used. The list of primers is described in Table 1. A variety of concentrations of myricetin-SLN-CS-FA were exposed to MCF-7 cells for 48 h. After incubating, a Biofact kit was used to extract the total RNA from the cells. In the following steps, RNA was evaluated using a nanodrop, cDNA was synthesized using RNA, and real-time qPCR was performed using Biorad-CFX96.

Assessment of antioxidant activities

The antioxidant activities of the myricetin-SLN-CS-FA were evaluated by DPPH, ABTS, and FRAP assay. To determine the inhibitory effect of free myricetin and myricetin-SLN-CS-FA on ABTS and DPPH free radicals, different concentrations of free myricetin and myricetin-SLN-CS-FA were prepared. Then an equal volume of the desired free radical was added to each microtube. Inhibition percentage was evaluated by substituting numbers in the following formula:

$$\% \text{ Free radicals scavenging } = \text{ OD Control} - \text{ OD Sample/OD Control} \times 100.$$

Free myricetin and myricetin-SLN-CS-FA reducing power was determined by measuring the iron chloride, TPTZ, and sodium acetate buffer concentrations in the FRAP reagent (10:1:1). A mixture of 20 ul of free myricetin and myricetin-SLN-CS-FA was mixed with 280 µl of FRAP reagent. After 10 min of incubation, the samples were measured for

Table 1 List of primers for real-time PCR

Test	Gene	Forward 5′–3′	Reverse 5′–3′
In vitro cytotoxic effect	Bax	TTTGCTTCAGGGTTTCATCCA	CTCCATGTTACTGTCCAGTTCGT
	Cas3	CTGGACTGTGGCATTGAGAC	ACAAAGCGACTGGATGAACC
	Cas9	CCAGAGATTCGCAAACCAGAGG	GAGCACCGACATCACCAAATCC
	Bcl-2	CATGTGTGTGGAGAGCGTCAAC	CAGATAGGCACCCAGGGTGAT
	GAPDH	TGCTGGTGCTGAGTATGTCG	GCATGTCAGATCCACAACGG
CAM assay	VEFG-A	GACCTGTAAATGTTCCTGCAA	AGAAATCAGGCTCCAGAAACA
	VEGFR-2	TCACGCCTTACAGACACCCT	AGGGAGATGTTACGGAGAATG
	β-actin	AGACAGCTACGTTGGTGATGAA	TGCTCCTCAGGGGCTACTCT
In vivo antitumor activity	TNFα	TTCTGTCTACTGAACTTCGGGGTGATCGGTCC	GTATGAGATAGCAAATCGGCTGACGGTGTGGG
	IL-6	CAAATTCGGTACATCCTC	CTGGCTTGTTCCTCACTA
	SOD	AGCATGGGTTCCACGTCCA	CACATTGGCCACACCGTCCT
	HER2	GCAGCTTCATGTCTGTGCC	ACAGAGACTCAGACCCTGGC

absorbance at 593 nm. The standard curve at 593 nm was prepared using different concentrations of FeSO4 (Tuekaew et al. 2014).

Chick chorioallantoic membrane (CAM) assay and in vivo gene expression analysis

The eggs were produced by Toos Mashhad Company and incubated at 37 °C in a humid environment of 55–70% for 48 h after disinfection. After incubation, a window was created by removing part of the eggshell and blocking it with paraffin and glue. On day 8, the glue and paraffin were removed, and a small portion of the gelatin sponge made from agar and egg white was placed on the membrane. The sponge was loaded with different concentrations of myricetin-SLN-CS-FA, and the eggshell was sealed. After 4 days in the incubator, the window in the shell was opened to image the gelatin sponge area, and the effects of treatment were evaluated. Calipers and scales were also used to measure fetal weight and height.

For gene expression analysis, Liquid nitrogen was used to pulverize the chorioallantoic membrane of each sample. In the following steps, total RNA from tissue samples was extracted, cDNA was synthesized as a template, real-time qPCR was performed, and the amount of VEGF and VEGFR gene expressions were evaluated. The sequences of primers are described in Table 1.

In vivo antitumor and histological evaluations

Female BALB/c mice (6–8 weeks old) were obtained from the Pasteur Institute of Iran, Tehran, Iran. Afterward, 100 µl of a TUBO cell suspension containing 3×10^5 cells in PBS were injected subcutaneously into the right flank of each animal. 7 days later, when the tumors were palpable, the samples were divided into four groups, including a control group that received PBS and three experimental groups, including free myricetin, SLN-25, and SLN-50. The formulations were then administrated using oral gavage for 26 days post tumor inoculation and every two days. There was a group of healthy mice in which no tumor inoculation was performed on them. The size and weight of tumor samples were recorded on the day of treatment. For histopathological examination and RNA extraction, mice were euthanized, and their tissues and tumors were isolated and transferred to 10% formalin and phosphate buffer, respectively. The liver and tumor tissues were stained using hematoxylin and eosin (H&E) staining and analyzed using light microscopy. The expression levels of superoxide dismutase (SOD) and interleukin-6 (IL-6) genes were also evaluated in the liver. The tumor tissue tissues assessed the expression levels of tumor necroses factor alpha (TNF-α) and human epidermal growth factor receptor 2 (HER2). The sequences of primers are described in Table 1. Tumor volume can be calculated by multiplying the length* width^2/2 (Alizadeh et al. 2018). All animal experiments were approved by the Institutional Ethical Committee and Research Advisory Committee of Islamic Azad University and all animal experiments and methods were carried out in accordance with the relevant guidelines and regulations approved by the ethical committee and ARRIVE guidelines (Percie du Sert et al. 2020).

Statistical analysis

All results were analyzed with three replications using GraphPad prism software version 9 (GraphPad Software, Inc., San Diego, CA, USA). One-way ANOVA was used to

examine the differences between statistical groups at significance. $p < 0.05$ was considered statistically significant.

Results

Characterization of myricetin-SLN-CS-FA

According to the DLS results (Fig. 1A), there were particles forming with hydrodynamic diameters of 310.6 nm and PDI of 0.22. Figure 1B shows that the zeta potential of the SLN-CS-FA was 30.0 ± 4.8 mV. Figure 2 shows the SEM micrograph of the SLN-CS-FA, which indicates the spherical morphology of the formulation. The amount of FA binding to the CS was calculated using HPLC, which was 55%. Figure 3A and B demonstrates the FTIR results of the myricetin-SLN and myricetin-SLN-CF-FA, respectively. Strong peaks at 1595 cm^{-1} (bending mode of UN–H vibration) and 1661 cm^{-1} (stretching vibrational frequency peak of UC = O) confirm that the FA-CS is formed and CS successfully modified SLN. The percentage of myricetin encapsulated in the myricetin-SLN-SF-FA was obtained by calculating the difference between the total myricetin added and the myricetin encapsulated in SLN using HPLC. The encapsulated efficiency was calculated at 83%.

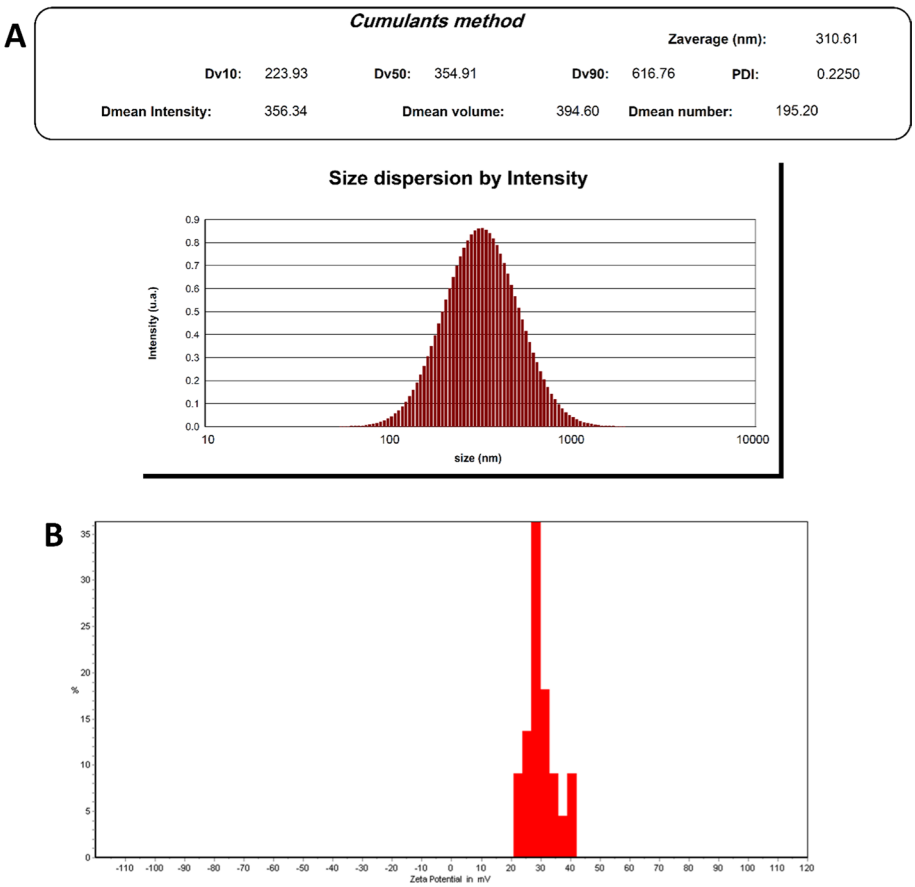

Fig. 1 Results of size and zeta potential. **A** The results of size by DLS demonstrated the size of 310 nm and PDI of 0.22 for myricetin-SLN-CS-FA. **B** The zeta potential of the myricetin-SLN-CS-FA was around + 30 mV

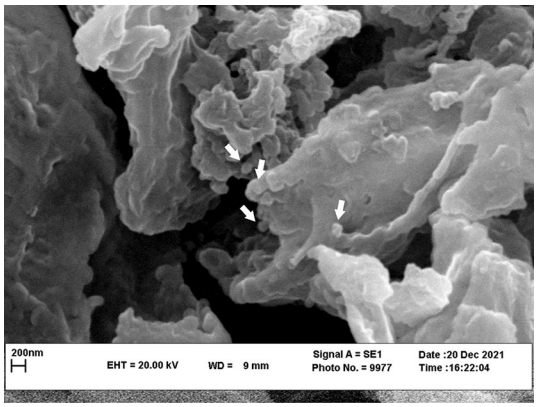

Fig. 2 Electron micrograph of the myricetin-SLN-CS-FA. The SEM image of the myricetin-SLN-CS-FA indicated the spherical morphology of the NPs (white arrow)

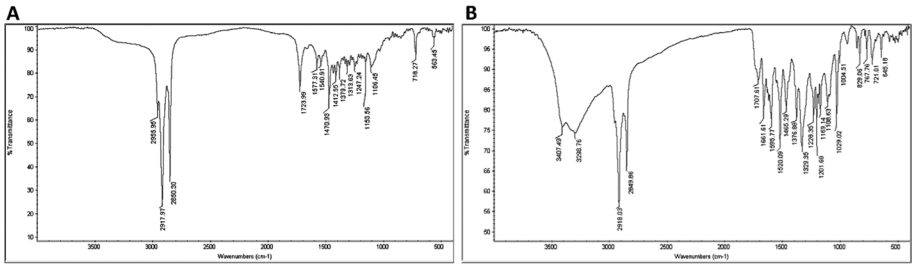

Fig. 3 FTIR spectrum. **A** The FTIR of the myricetin-SLN, which demonstrated the successful coating and **B** the FTIR of the myricetin-SLN-CS-FA The presence of strong peaks at 1595 cm^{-1} (bending mode of UN–H vibration) and 1661 cm^{-1} (stretching vibrational frequency peak of UC=O) confirm that the FA-CS is formed and CS successfully modified SLN

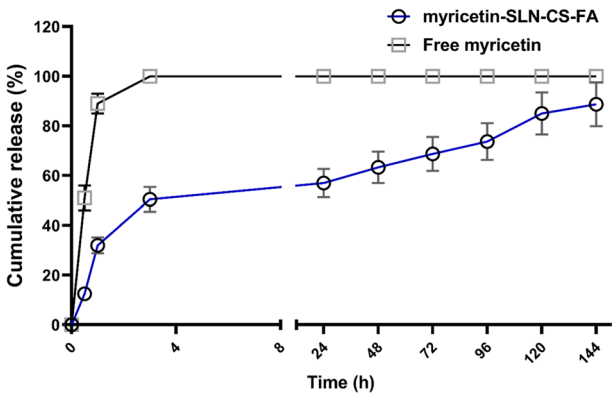

Fig. 4 Release study. The release profile of free myricetin and myricetin-SLN-CS-FA. The release study was performed in PBS until 144 h. The data are presented as mean ± SEM. The test was performed in triplicate

Release study

Figure 4 shows the release profile of free myricetin and myricetin from SLN-CS-FA nanoparticles. After 144 h, the cumulative release percentage of the drug is 88.7%. The initial burst release occurs in the early hours, and then the release pattern plateaus

until 144 h have passed. Based on the drug release kinetics and mechanism models, the myricetin-SLN-CS-FA release pattern was fitted by the Michaelis–Menten model with lag during 144 h of the study. Drug release rate from an aqueous solution of free myricetin was very quick, and after 3 h all of the drug completely moved across the dialysis bag.

Cytotoxicity study

MTT method was used to evaluate the anticancer activity of free myricetin for 48 h against MCF-7 cells and myricetin-SLN-CS-FA during 24, 48, and 72 h against HFF and MCF-7-NCF-NPs against MCF-7 cancer cells. Figure 5 shows the inhibitory effect of free myricetin in a concentration-dependent manner. Then, the carcinogenic effect of myricetin-SLN-CS-FA against HFF and MCF-7 cells is shown in Fig. 6A and B. As demonstrated, the myricetin-SLN-CS-FA had no cytotoxic effects against HFF normal cells, while the cytotoxicity of formulation against MCF-7 cells was in a time- and concentration-dependent manner. At concentrations of 6.25, 12.5 and 25 µg/ml the differences with cells without treatment at 48 and 72 h were significant ($^{*}p < 0.05$ and $^{***}p < 0.001$), while at concentrations of 50 and 100 µg/ml the differences of 24, 48 and 72 h were statistically significant ($^{***}p < 0.001$).

Anti-apoptotic study

By studying the cell cycle using flow cytometry, myricetin-SLN-CS-FA inhibited cell growth and proliferation. With increasing concentrations of myricetin-SLN-CS-FA, the effect of the treatment on cell cycle arrest in the SubG1 phase increases (Fig. 7A–D). It can be seen that in the control sample, only 2.5% of the cells are in the SubG1 phase, whereas in the treated samples at concentrations of 25, 35, and 45 µg/ml of myricetin-SLN-CS-FA, 29, 54, and 79% of the cells are in the SubG1 phase. It has been confirmed that myricetin-SLN-CS-FA induces apoptosis in treated cells.

Based on the results of the AO/PI analysis, it is evident that cells treated with myricetin-SLN-CS-FA at various concentrations exhibit cytotoxic and apoptotic effects (Fig. 8). These treated cells exhibit morphological changes, such as a reduction in size and a change in shape to a spherical shape, which are characteristics of apoptotic cells. The

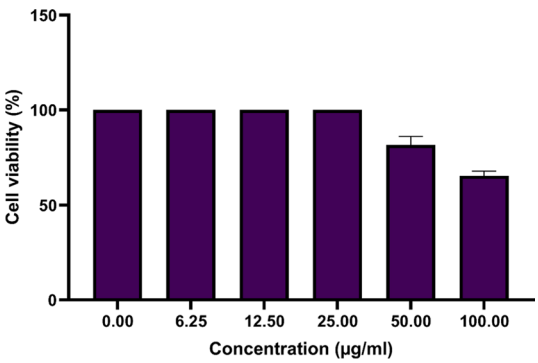

Fig. 5 Cytotoxicity of the free myricetin. The cytotoxicity effects of free myricetin against the MCF-7 cell line were evaluated in which the cells were killed in a concentration-dependent manner. The data are presented as mean ± SEM. The test was performed in triplicate

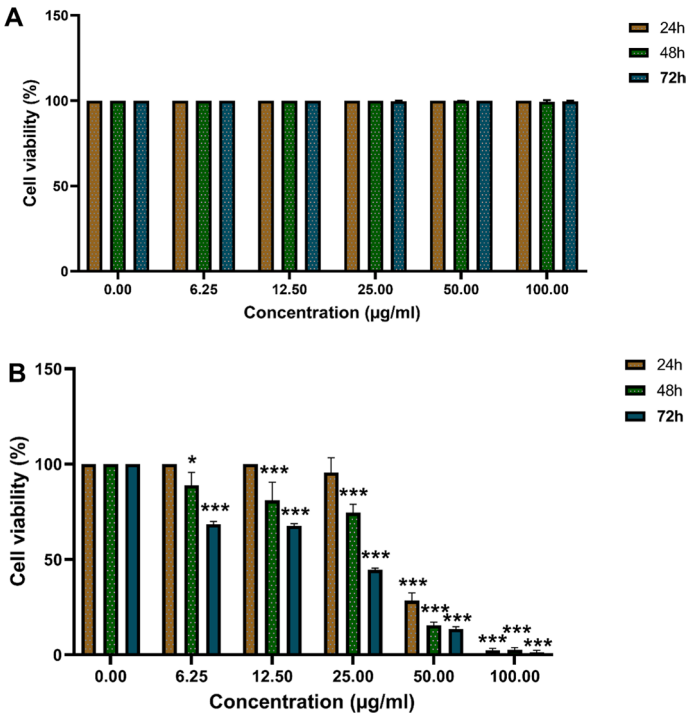

Fig. 6 Cytotoxicity of the myricetin-SLN-CS-FA during 72 h. **A** The cytotoxicity effects of myricetin-SLN-CS-FA against the HFF cell line were evaluated. No sign of cytotoxicity was observed in these concentrations and the study times. **B** The cytotoxicity effects of myricetin-SLN-CS-FA against the MCF-7 cell line were evaluated in which the cells were killed in a concentration and time-dependent manner. The data are presented as mean ± SEM. The test was performed in triplicate. (*$p < 0.05$ and ***$p < 0.001$)

images also show germination of the plasma membrane and shrinkage of the cells. Control cells emit uniform green fluorescence from the nucleus and cytoplasm, indicating that the cells have not undergone any morphological changes. In contrast, treated cells emit red fluorescence, which means the penetration of the PI dye into damaged cells increases the incidence of apoptosis as the concentration of the treatment increases. Fluorescence microscopy and the DAPI method confirmed the change in density and fragmentation of the nucleus in the treated cells. As the concentration of treatment increases, bright spots indicate the nuclei of apoptotic cells. Apoptosis increases as treatment concentration increases, as shown in these images.

Real-time qPCR

It has been shown that the expression of the studied genes has changed over time, which indicates that the internal apoptosis pathway of the cells has been activated (Fig. 9). An apoptotic mechanism of action for myricetin-SLN-CS-FA can be described as follows: treatment with myricetin-SLN-CS-FA has been associated with an increase in Bax, Cas3, and Cas9 gene expression and a decrease in Bcl-2 gene expression, leading to the release of cytochrome C from the mitochondria into the cytoplasm. There is evidence that increased levels of cytoplasmic cytochrome are associated with activation of caspase-dependent downstream pathways, promoting intrinsic apoptosis.

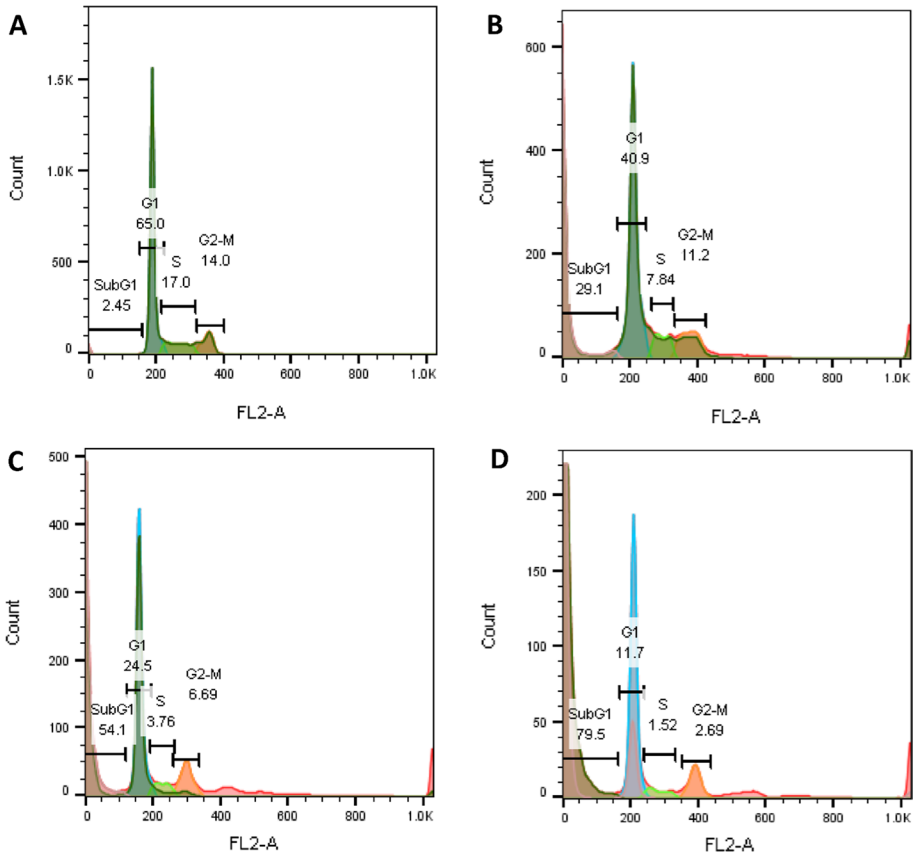

Fig. 7 Apoptosis analysis with flow cytometry. Increasing the percentage of SubG1 phase cells indicates the occurrence of apoptosis in MCF-7 cells treated with myricetin-SLN-CS-FA. **A** control without treatment, **B** 25 µg/ml, **C** 35 µg/ml, and **D** 45 µg/ml of the myricetin-SLN-CS-FA

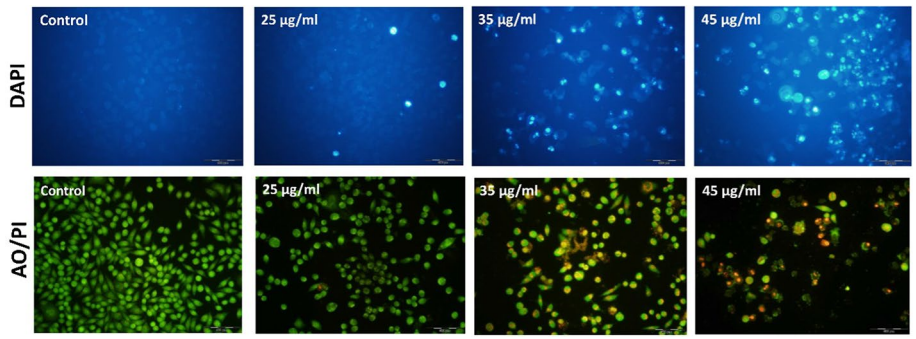

Fig. 8 **A** DAPI and **B** AO/PI staining of MCF-7 cells treated with different concentrations (25, 35, and 45 µg/ml) of myricetin-SLN-CS-FA

Assessment of antioxidant activities

As can be seen in Fig. 10A and B, free myricetin and myricetin-SLN-CS-FA inhibit the oxidative stress caused by free radicals such as ABTS and DPPH. ABTS free radicals as well as DPPH free radicals, can be inhibited by free myricetin and myricetin-SLN-CS-FA in a concentration-dependent manner. The results below show how myricetin-SLN-CS-FA is more effective at inhibiting ABTS radicals with a higher power than

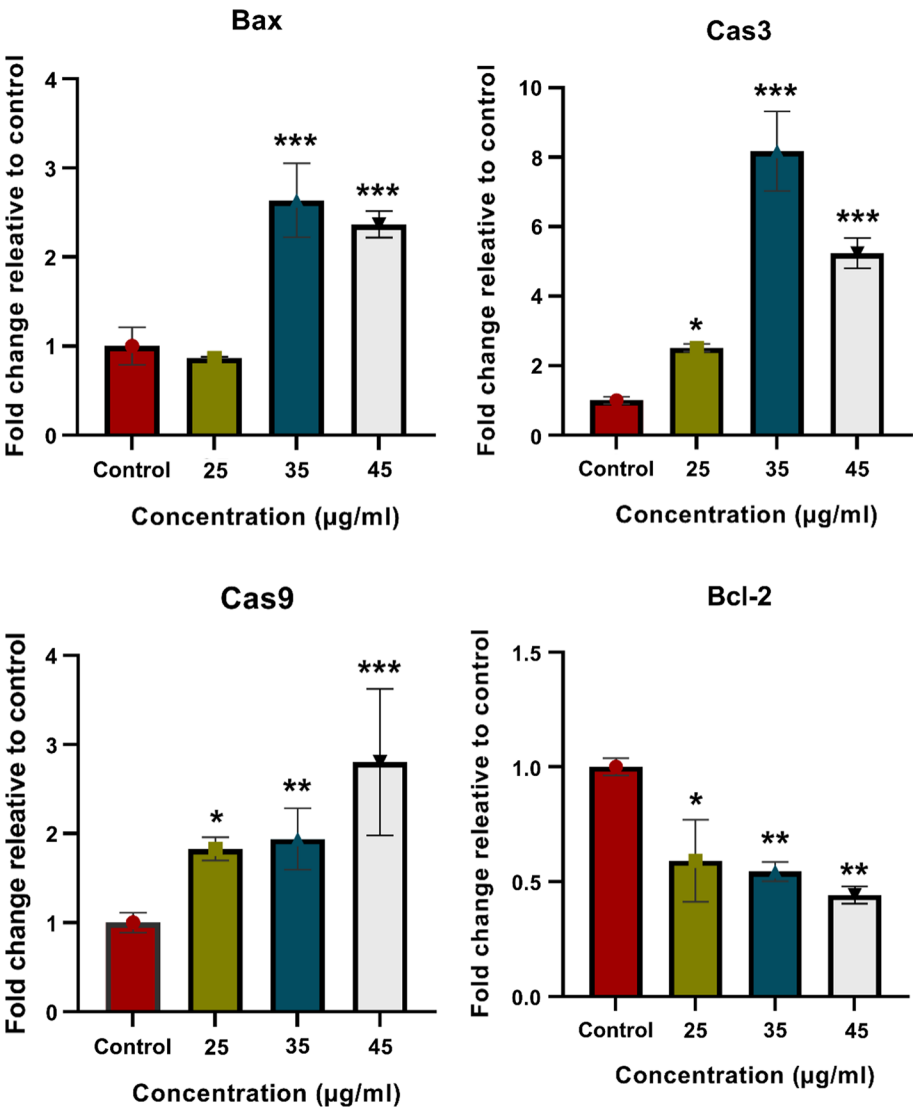

Fig. 9 Quantitative analysis of Bax, Cas3, Cas9, and Bcl-2 genes expression as pro-apoptotic factors (*$p < 0.05$, **$p < 0.01$, and ***$p < 0.001$). The data were presented as mean ± SD. The test was performed in triplicate

DPPH. As a result of these findings, it appears that nanoparticles have an antioxidant effect in vitro.

Figure 10C and D illustrates how free myricetin and myricetin-SLN-CS-FA is capable of reducing iron ions compared to FeSO4. It can be seen from the diagram that the FRAP value increases with increasing concentration of myricetin-SLN-CS-FA, and the highest amount of FRAP value (0.68) was obtained when the concentration of myricetin-SLN-CS-FA was 2 µg/ml. The capabilities of the free myricetin in reducing iron ions was weaker than myricetin-SLN-CS-FA.

CAM assay and in vivo gene expression

A microscopic examination of the treated area confirms that the number of blood vessels has decreased (Fig. 11A). Myricetin-SLN-CS-FA showed significant anti-angiogenesis

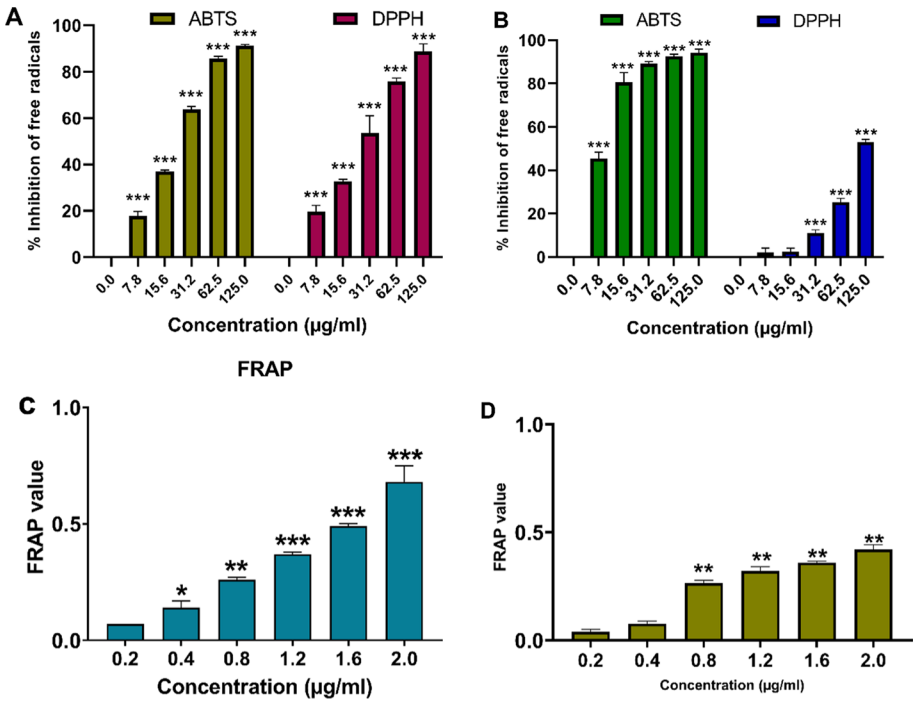

Fig. 10 Myricetin-SLN-CS-FA antioxidant activity. **A** Scavenging effects of myricetin-SLN-CS-FA on ABTS and DPPH free radicals, and **B** scavenging effects of free myricetin on ABTS and DPPH free radicals. **C** Ferric reducing antioxidant power (FRAP) of myricetin-SLN-CS-FA and **D** ferric reducing antioxidant power (FRAP) of free myricetin (*$p < 0.05$, **$p < 0.01$, and ***$p < 0.001$). The data were presented as mean ± SD. The test was performed in triplicate

effects in all three concentrations when compared with the control and laboratory control groups. Using Image J software, the number and length of blood vessels were quantitatively analyzed. Data analysis showed no statistically significant difference between the control and lab control groups. In contrast, in all three groups treated with concentrations of 250, 500, and 1000 µg/ml, a significant decrease (***$p < 0.001$) in the number and length of blood vessels was observed compared to the control (Fig. 11B, C). Myricetin-SLN-CS-FA-treated samples showed changes in embryonic growth factors compared to control samples in length and weight measurements (Fig. 11D, E). Among control, lab control, and treated samples, the differences in embryo lengths were statistically significant (*$p < 0.05$. **$p < 0.01$, and ***$p < 0.001$).

The expression of VEGF and VEGFR is crucial for the formation and germination of blood vessels. As shown in Fig. 11F, both genes were expressed less in the samples treated with myricetin-SLN-CS-FA. The rate of reduction of both genes in all experimental groups was significant compared to the control (**$p < 0.01$ and ***$p < 0.001$).

In vivo antitumor activities

Figure 12A and B shows the effects of formulations on the tumor volume and animal weight, respectively. As indicated, both doses of myricetin-SLN-CS-FA (25 and 50 µg/kg) showed significant effects in the treatment groups than the free myricetin ($p < 0.05$), indicating that the formulation was more effective in inhibiting tumor growth than the free form of the drug. As shown, the weight of no animal fell below

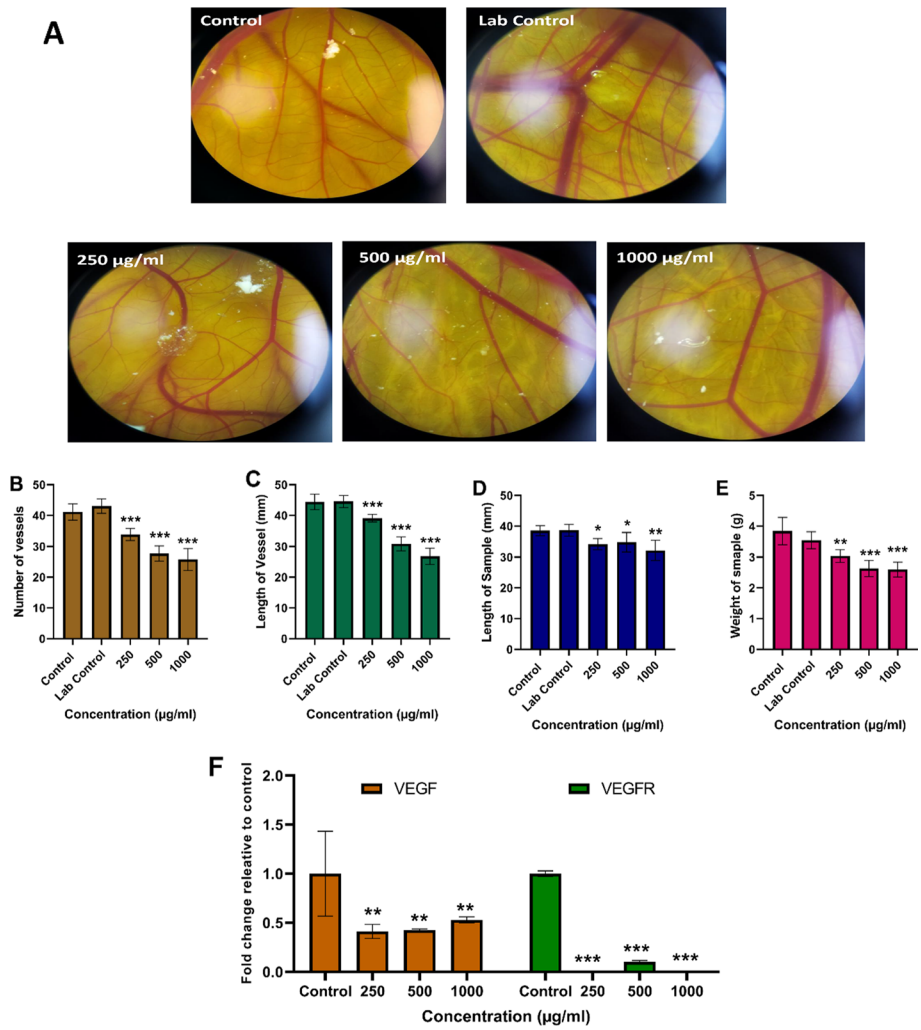

Fig. 11 CAM assay. **A** Stereomicroscopic images of chorioallantoic membrane vessels in treatment with myricetin-SLN-CS-FA compared to control. **B**–**E** Significant reduction in mean length and number of blood vessels along with a reduction in embryonic growth factors in myricetin-SLN-CS-FA treated samples. **F** The effects of myricetin-SLN-CS-FA on VEGF and VEGFR gene expressions (*$p < 0.05$, **$p < 0.01$, and ***$p < 0.001$). The data were presented as mean ± SD. The test was performed in triplicate

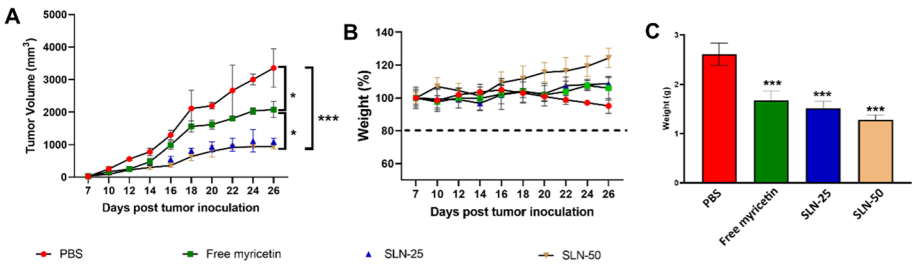

Fig. 12 Antitumor activities of myricetin-SLN-CS-FA on mice bearing subcutaneous TUBO cells tumor model treated with free myricetin and two doses of myricetin-SLN-CS-FA (25 and 50 mg/kg) which administrated using oral gavage. **A** The results of tumor volume during the 26 days of the study. **B** The results of animal weights during the 26 days of the study. **C** The weights of the tumor tissues on day 26 after tumor inoculation (*$p < 0.05$ and ***$p < 0.001$). The data were presented as mean ± SD. The test was performed in triplicate

80% of the initial weight. On day 26, the tumors were removed and weighted. The results also indicated that the weights of the tumors were significantly decreased in all treatment groups compared to the control group (see Fig. 12C). According to the H&E staining images on healthy liver samples (Fig. 13), the treated groups showed no pathology changes, indicating no toxicity of myricetin-SLN-CS-FA on cells. A comparison of tumor samples in the control group (untreated) and the treated group (treated) showed significant tissue changes. Apoptotic cells appear dark, spherical, and small in the treated samples. As myricetin-SLN-CS-FA concentrations increase, more apoptotic islets are present, indicating that the treatment is effective. Figure 14A shows the results of gene expression for IL-6 and SOD in the tumor tissues, which demonstrated the highest levels of the expression of both genes in the free myricetin group, while these expressions were the lowest in the SLN-50 ($p < 0.001$). In the liver (Fig. 14B), there was the lowest expression of the TNF-α and HER2 which were statistically significant ($p < 0.001$).

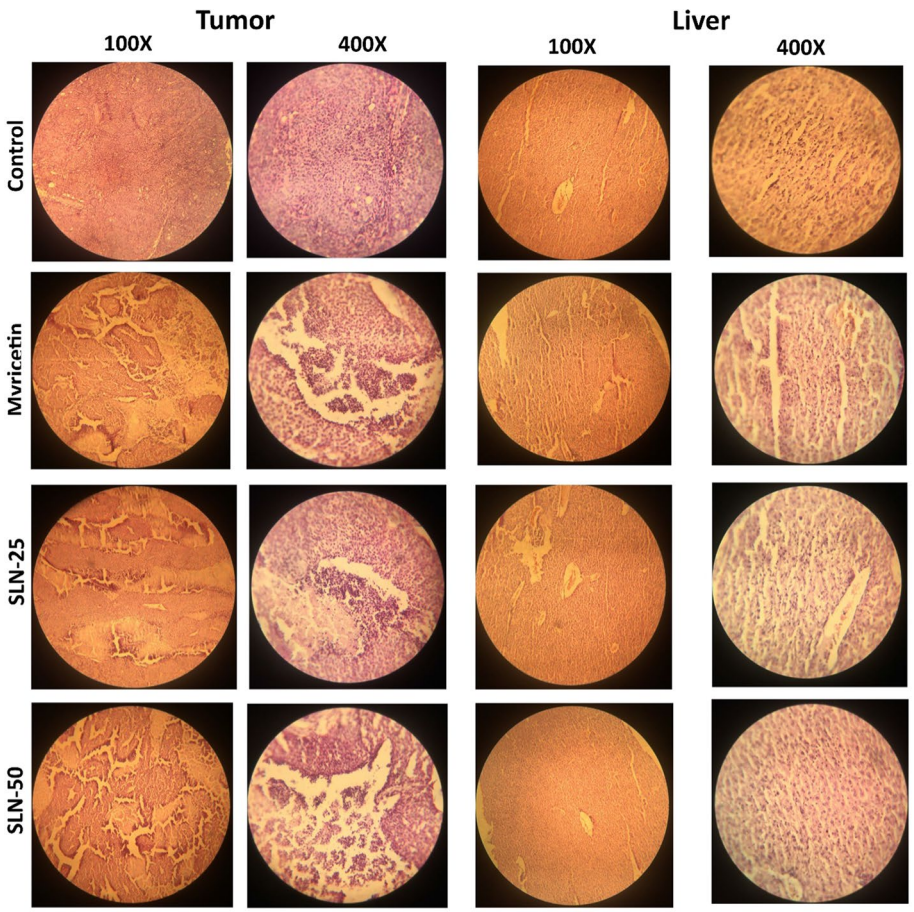

Fig. 13 H&E staining of liver and tumor from TUBO tumor model, which subcutaneously inoculated in the right flank of mice. The animals were treated with free myricetin and doses of 25 and 50 mg/kg of myricetin-SLN-CS-FA (SLN-25 and SLN-50). The samples were investigated under 100× and 400× magnification fields

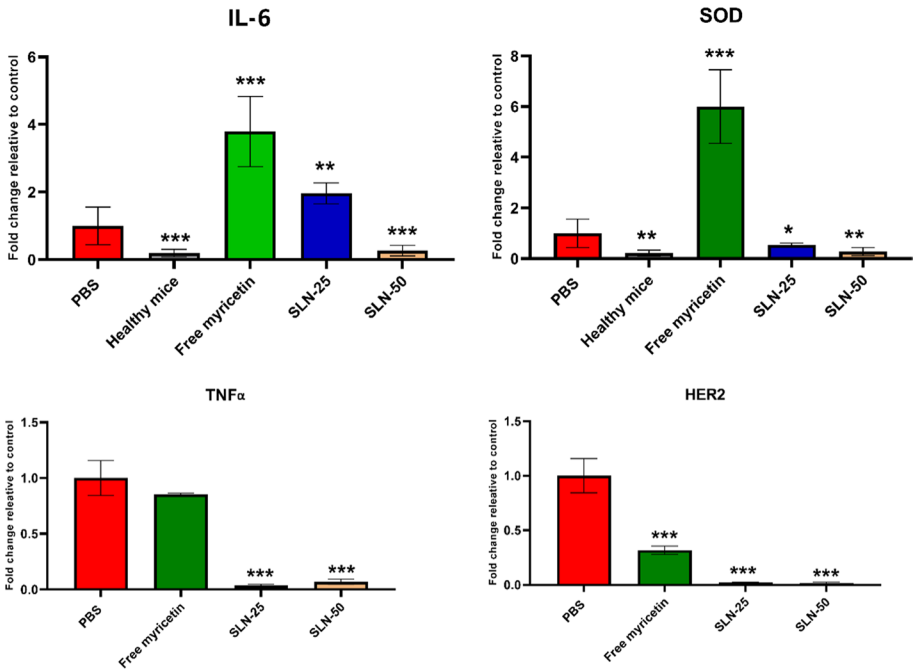

Fig. 14 Changes in the expression of inflammatory and antioxidant genes from the liver (IL-6 and SOD) and tumor (TNFα and HER2). The expression levels of IL-6 and SOD were also compared with healthy mice with no tumors (*$p < 0.05$, $p < 0.01$, and ***$p < 0.001$). The data were presented as mean ± SD. The test was performed in triplicate

Discussion

This study examined using FA-bound CS to modify the myricetin-containing containing SLN. As a result of its cationic nature, CS significantly improves the internalization of drugs into cancer cells due to its ability to change the surface charge of NPs from negative to positive (Ying et al. 2011). Alternatively, FA can target FA receptors on the surface of cancer cells and increase cell uptake and treatment efficacy (Monteiro et al. 2020).

SLN was used in the current study to encapsulate myricetin. Then the formulation was surfaces modified using CS and active-targeted with FA. A high entrapment efficiency 83%, a particle size of 310 nm, and a positive zeta potential value were obtained based on measurements of particle size and entrapment efficiency. SEM illustrates the spherical shape of the particles. Nanoparticles synthesized in this study had a PDI of 0.22. A particle's average diameter and PDI play an essential role in the stability of a formulation. In other words, particles with smaller diameters and narrow distribution ranges are more stable and have a slight tendency to aggregate (Bahari and Hamishehkar 2016). In the preparation of SLNs for the delivery of myricetin, stearic acid could be used as a matrix material. Stearic acid, as an antioxidant, is an ideal material for use in SLNs. Stearic acid has a melting point of 69.6 °C. It is possible to use stearic acid as a lipid matrix material in nanoparticles because its melting point is much higher than that of the human body (Kumar and Randhawa 2015). Here lecithin and Tween 80 were used as emulsifiers and helped the formation of the SLN and higher EE% of the drug (Luo et al. 2006).

In this study, CS has been used to surface-modify the SLNs due to its low toxicity, good biocompatibility, and absorption-enhancing properties (Sogias et al. 2008). The coating

with CS, a natural cationic polysaccharide derived from chitin by partially deacetylating its acetamide groups, to nanoparticle surfaces might increase drug penetration in cells, especially in mucosal surfaces (Fonte et al. 2011). Furthermore, the high binding affinity of FA for the FRs, which are overexpressed on human adenocarcinoma (MCF-7) cells, makes it an attractive target ligand. The functionalization of SLN with FA has been proposed as an active tumor targeting strategy. FA binds to the FR on tumor cells, resulting in its internalization by receptor-mediated endocytosis (Granja et al. 2022). Here the FA was bound to the CS using EDC/NHS coupling chemistry and then decorated on the surface of SLN. The results of HPLC indicated that the binding efficiency was 55%, and the surface modification was confirmed using FTIR. The results of the present study are inconsistent with the results of a study that used FA as an active targeting ligand on the surface of SLN, which was confirmed by FTIR (Pawar et al. 2016).

The release of myricetin from SLN was evaluated during 144 h. The results demonstrated the burst release (50%) of myricetin during the first 4 h, followed by the plateau pattern until 144 h. the kinetic analysis indicated that the Michaelis–Menten model with lag fitted the release of myricetin from the SLN. In some cases, burst release is an optimal delivery method. To exert gradual anticancer effects, as demonstrated by the release study, some drugs require an initial burst followed by a prolonged release, producing an immediate dose and a prolonged release (Cam et al. 2020).

The results of this study showed that free myricetin has cytotoxic activity against the MCF-7 cell line. It was suggested that myricetin exerts cytotoxic activity through binding to the oncogene Moloney murine leukemia virus 1 (PIM-1) binding site and inhibiting its kinase activity (Ye et al. 2018). In breast cancer, particularly in triple-negative tumors, the oncogene PIM-1 is upregulated. Furthermore, it contributes to tumorigenesis, drug resistance, and poor prognoses (Chen and Tang 2019). The cytotoxicity effects of myricetin-SLN-CS-FA were investigated against HFF normal and MCF-7 carcinoma cells. The results demonstrated the cytotoxic effects of formulations against MCF-7 cells, whereas the formulation had no cytotoxic effects against normal cells at the corresponding concentrations. These results indicated that formulating the myricetin in the form of SLN could protect normal cells against cytotoxic effects of myricetin up to 100 μg/ml concentration. The possibility of this formulation reducing the adverse effects of the drug at the cellular level is worth considering (Patra et al. 2018).

Flow cytometry showed that the cells treated with myricetin-SLN-CS-FA significantly increased in the subG1 phase compared to the control. The cells exposed to the SLNs had a higher rate of apoptosis. Additionally, the subG1 peak intensified as the SLN concentration increased. Compared to lower concentrations, 35 μg/ml dramatically increased the rate of apoptotic cells, showing dose-dependent effects. As demonstrated by the fluorescent staining of the myricetin-SLN-CS-FA in the current study, the myricetin-SLN-CS-FA induced apoptosis dose-dependently. An AO/PI fluorescent microscopic image revealed morphological changes such as shrinkage of cells, fragmentation of nuclear nuclei, condensation of chromatin, and membrane blebbing indicative of apoptosis (Sharifalhoseini et al. 2021; Zhang et al. 2018b).

Cell proliferation and death are interdependent, so inducing apoptosis could be a valuable strategy for treating cancer. The cancer cells, however, have developed numerous mechanisms to resist apoptosis. The cancer cells, however, have developed numerous

mechanisms to resist apoptosis. Apoptosis resistance is caused by the overexpression of anti-apoptotic Bcl2 family proteins, which decreases the effectiveness of therapeutics. In mitochondrial cells, the Bcl2 family of proteins regulates intrinsic apoptosis. Bcl2 inhibits the formation of pores and the release of cytochrome c by binding to pro-apoptotic members like Bax.

On the other hand, the increase in expression of Bax results in the elimination of tumor cells as a result of cell death. Our results supported that myricetin-SLN-CS-FA induces mitochondrial apoptosis through the Bcl2 and Bax proteins, which have been implicated in many tumor cells (Naseri et al. 2015). As a result of oxidative stress, ROS are produced in the cell, or the redox balance is disrupted, which promotes apoptosis and interferes with cell proliferation. Caspases and HSP70 are vital components of apoptosis in mammals (Ramesha et al. 2015). As demonstrated here, myricetin treatment of cells at 25–45 μg/ml increased gene expression of apoptosis-inducing proteins and enzymes such as Cas3 and Cas9 mRNA levels in a dose-dependent manner.

ABTS and DPPH free radicals were inhibited by myricetin-SLN-CS-FA in vitro (Fig. 10A) and FRAP free radicals (Fig. 10B), indicating the antioxidant activity of the formulation. Myricetin-SLN-CS-FA can inhibit free radicals and prevent oxidative damage in natural conditions but is pro-oxidant in cancer cells and can induce apoptosis (Soltani et al. 2021).

Study results in the CAM model showed that myricetin-SLN-CS-FA inhibited the growth of blood vessels, as well as inhibiting the production of embryonic growth factors. Study findings showed that myricetin-SLN-CS-FA treatment decreased the expression of angiogenesis-related genes (VEGF and VEGF-R). In all parameters, including the number and length of blood vessels and the length and weight of the embryos, all concentrations of myricetin-SLN-CS-FA significantly showed anti-angiogenic activities. It was demonstrated that myricetin induces apoptosis and procaspase-3 cleavage by generating reactive oxygen species (ROS). A significant reduction in PI3K/Akt/mTOR signaling was observed in HUVECs following treatment with this compound, which indicated its anti-angiogenic activity (Kim 2017). As shown here, the reduction in expression levels of VEGF and VEGFR, the genes involved in angiogenesis, indicated the anti-angiogenesis effects of formulation.

The antitumor activity study showed that in both doses of 25 and 50 mg/kg of the myricetin-SLN-CS-FA, there was a decline in the tumor volume compared to the free myricetin and control group. In addition, both doses had no significant effects on the animal weights, implying the safety of these doses (Mashreghi et al. 2021). The tumor weights' results also indicated the formulation's antitumor activities in decreasing tumor growth rates in both doses of myricetin-SLN-CS-FA-25 and -50 (Mirzavi et al. 2022). The H&E staining of tumor tissues also indicated the antitumor activities of myricetin-SLN-CS-FA on histological parameters of tissue, in which histological damage and dark apoptotic and necrotic sites were observable (Katifelis et al. 2020). No signs of pathohistological damage in the livers of all groups also indicated the safety of the formulations (El-Sayyad et al. 2009). Compared with free myricetin, myricetin-SLN-CS-FA reduced inflammatory and antioxidant gene expression in the treated samples' livers. In addition, myricetin-SLN-CS-FA reduced expression levels of TNF-alpha and HER2 in tumors, decreasing the inflammatory response (Semwal et al. 2016; Chen et al. 2020).

Conclusion

In the present work, myricetin-SLN decorated with FA-bound CS was prepared by homogenizing and ultrasonically mixing. Myricetin-SLN-CS-FA was evaluated in vitro and in vivo and showed higher toxicity on cancer cells than on free myricetin. Apoptotic genes were altered, and antioxidant gene expression decreased in treated cells, confirming the activation of the intrinsic apoptotic pathway. A CAM method and molecular analysis confirmed the anti-angiogenesis effects of myricetin-SLN-CS-FA, and histopathological staining and molecular analysis confirmed the antitumor impact of myricetin-SLN-CS-FA in vivo. Based on our in vitro and in vivo findings, myricetin-SLN-CS-FA is effective in treating breast cancer, and this formulation can be recommended for further studies.

Acknowledgements
This work was supported by, Islamic Azad University, Neyshabur, Iran, and thus is appreciated by the author.

Author contributions
NK: methodology, investigation and writing—original draft. AM and MHT: supervision, data curation, conceptualization and writing—reviewing and editing. RZ: formal analysis, software. JM: validation, investigation. All authors read and approved the final manuscript.

Funding
This research was performed at personal expense in the laboratory of Islamic Azad University of Neyshabur.

Availability of data and materials
The datasets used and/or analyzed during the current study are available from the corresponding author upon reasonable request.

Declarations

Ethics approval and consent to participate
All institutional and national guidelines for the care and use of laboratory animals were followed.

Consent for publication
Not applicable.

Competing interests
The authors declare that they have no competing interests.

Received: 18 December 2022 Accepted: 31 January 2023
Published online: 06 February 2023

References

Alhajamee M, Marai K, Al Abbas SMN, Homayouni Tabrizi M (2021) Co-encapsulation of curcumin and tamoxifen in lipid-chitosan hybrid nanoparticles for cancer therapy. Mater Technol 89:1–12
Alizadeh MN, Rashidi M, Muhammadnejad A, Zanjani TM, Ziai SA (2018) Antitumor effects of umbelliprenin in a mouse model of colorectal cancer. Iran J Pharma Res 17(3):976
Bahari LAS, Hamishehkar H (2016) The impact of variables on particle size of solid lipid nanoparticles and nanostructured lipid carriers; a comparative literature review. Advan Pharma Bull 6(2):143
Cam ME, Yildiz S, Alenezi H, Cesur S, Ozcan GS, Erdemir G, Edirisinghe U, Akakin D, Kuruca DS, Kabasakal L (2020) Evaluation of burst release and sustained release of pioglitazone-loaded fibrous mats on diabetic wound healing: an in vitro and in vivo comparison study. J R Soc Interface 17(162):20190712
Cao J, Chen H, Lu W, Wu Y, Wu X, Xia D, Zhu J (2018) Myricetin induces protective autophagy by inhibiting the phosphorylation of mTOR in HepG2 cells. Anat Rec 301(5):786–795
Chen J, Tang G (2019) PIM-1 kinase: a potential biomarker of triple-negative breast cancer. Onco Targets Ther 12:6267
Chen M, Chen Z, Huang D, Sun C, Xie J, Chen T, Zhao X, Huang Y, Li D, Wu B (2020) Myricetin inhibits TNF-α-induced inflammation in A549 cells via the SIRT1/NF-κB pathway. Pulm Pharmacol Ther 65:102000
El-Sayyad HI, Ismail MF, Shalaby F, Abou-El-Magd R, Gaur RL, Fernando A, Raj MH, Ouhtit A (2009) Histopathological effects of cisplatin, doxorubicin and 5-fluorouracil (5-FU) on the liver of male albino rats. Int J Biol Sci 5(5):466
Feng J, Chen X, Wang Y, Du Y, Sun Q, Zang W, Zhao G (2015) Myricetin inhibits proliferation and induces apoptosis and cell cycle arrest in gastric cancer cells. Mol Cell Biochem 408(1):163–170
Fernández M, Javaid F, Chudasama V (2018) Advances in targeting the folate receptor in the treatment/imaging of cancers. Chem Sci 9(4):790–810

Fonte P, Nogueira T, Gehm C, Ferreira D, Sarmento B (2011) Chitosan-coated solid lipid nanoparticles enhance the oral absorption of insulin. Drug Deliv Transl Res 1(4):299–308
Granja A, Nunes C, Sousa CT, Reis S (2022) Folate receptor-mediated delivery of mitoxantrone-loaded solid lipid nanoparticles to breast cancer cells. Biomed Pharmacother 154:113525
Hamedinasab H, Rezayan AH, Mellat M, Mashreghi M, Jaafari MR (2020) Development of chitosan-coated liposome for pulmonary delivery of N-acetylcysteine. Int J Biol Macromol 156:1455–1463
Katifelis H, Mukha I, Bouziotis P, Vityuk N, Tsoukalas C, Lazaris AC, Lyberopoulou A, Theodoropoulos GE, Efstathopoulos EP, Gazouli M (2020) Ag/Au bimetallic nanoparticles inhibit tumor growth and prevent metastasis in a mouse model. Int J Nanomed 15:6019
Kim GD (2017) Myricetin inhibits angiogenesis by inducing apoptosis and suppressing PI3K/Akt/mTOR signaling in endothelial cells. J Cancer Prev 22(4):219
Kumar S, Randhawa JK (2015) Solid lipid nanoparticles of stearic acid for the drug delivery of paliperidone. RSC Adv 5(84):68743–68750
Luo Y, Chen D, Ren L, Zhao X, Qin J (2006) Solid lipid nanoparticles for enhancing vinpocetine's oral bioavailability. J Control Release 114(1):53–59
Mashreghi M, Azarpara H, Bazaz MR, Jafari A, Masoudifar A, Mirzaei H, Jaafari MR (2018) Angiogenesis biomarkers and their targeting ligands as potential targets for tumor angiogenesis. J Cell Physiol 233(4):2949–2965
Mashreghi M, Faal Maleki M, Karimi M, Kalalinia F, Badiee A, Jaafari MR (2021) Improving anti-tumour efficacy of PEGylated liposomal doxorubicin by dual targeting of tumour cells and tumour endothelial cells using anti-p32 CGKRK peptide. J Drug Target 29(6):617–630
Mirzavi F, Barati M, Vakili-Ghartavol R, Roshan MK, Mashreghi M, Soukhtanloo M, Jaafari MR (2022) Pegylated liposomal encapsulation improves the antitumor efficacy of combretastatin A4 in murine 4T1 triple-negative breast cancer model. Int J Pharm 613:121396
Monteiro CA, Oliveira AD, Silva RC, Lima RR, Souto FO, Baratti MO, Carvalho HF, Santos BS, Cabral Filho PE, Fontes A (2020) Evaluating internalization and recycling of folate receptors in breast cancer cells using quantum dots. J Photochem Photobiol 209:111918
Naseri MH, Mahdavi M, Davoodi J, Tackallou SH, Goudarzvand M, Neishabouri SH (2015) Up regulation of Bax and down regulation of Bcl2 during 3-NC mediated apoptosis in human cancer cells. Cancer Cell Int 15(1):1–9
Nasirizadeh S, Malaekeh-Nikouei B (2020) Solid lipid nanoparticles and nanostructured lipid carriers in oral cancer drug delivery. J Drug Deliv Sci Technol 55:101458
Patra JK, Das G, Fraceto LF, Campos EVR (2018) Nano based drug delivery systems: recent developments and future prospects. J Nanobiotechnol 16(1):1–33
Pawar H, Surapaneni SK, Tikoo K, Singh C, Burman R, Gill MS, Suresh S (2016) Folic acid functionalized long-circulating co-encapsulated docetaxel and curcumin solid lipid nanoparticles: in vitro evaluation, pharmacokinetic and biodistribution in rats. Drug Delivery 23(4):1453–1468
Percie du Sert N, Hurst V, Ahluwalia A, Alam S, Avey MT, Baker M, Browne WJ, Clark A, Cuthill IC, Dirnagl U (2020) The ARRIVE guidelines 2.0: Updated guidelines for reporting animal research. J Cerebral Blood Flow Metab 40(9):1769–1777
Rahmati A, Homayouni Tabrizi M, Karimi E, Zarei B (2022) Fabrication and assessment of folic acid conjugated-chitosan modified PLGA nanoparticle for delivery of alpha terpineol in colon cancer. J Biomater Sci 89:1–19
Ramesha A, Venkataramana M, Nirmaladevi D, Gupta VK, Chandranayaka S, Srinivas C (2015) Cytotoxic effects of oosporein isolated from endophytic fungus Cochliobolus kusanoi. Front Microbiol 6:870
Sandri G, Bonferoni MC, Gökçe EH, Ferrari F, Rossi S, Patrini M, Caramella C (2010) Chitosan-associated SLN: in vitro and ex vivo characterization of cyclosporine A loaded ophthalmic systems. J Microencapsul 27(8):735–746
Sarkar S, Horn G, Moulton K, Oza A, Byler S, Kokolus S, Longacre M (2013) Cancer development, progression, and therapy: an epigenetic overview. Int J Mol Sci 14(10):21087–21113
Semwal DK, Semwal RB, Combrinck S, Viljoen A (2016) Myricetin: A dietary molecule with diverse biological activities. Nutrients 8(2):90
Sharifalhoseini M, Es-haghi A, Vaezi G, Shajiee H (2021) Biosynthesis and characterisation of solid lipid nanoparticles and investigation of toxicity against breast cancer cell line. IET Nanobiotechnol 15(8):654–663
Shiomi K, Kuriyama I, Yoshida H, Mizushina Y (2013) Inhibitory effects of myricetin on mammalian DNA polymerase, topoisomerase and human cancer cell proliferation. Food Chem 139(1–4):910–918
Sogias IA, Williams AC, Khutoryanskiy VV (2008) Why is chitosan mucoadhesive? Biomacromol 9(7):1837–1842
Soltani M, Parivar K, Baharara J, Kerachian MA, Asili J (2015) Putative mechanism for apoptosis-inducing properties of crude saponin isolated from sea cucumber (Holothuria leucospilota) as an antioxidant compound. Iran J Basic Med Sci 18(2):180
Soltani M, Etminan A, Rahmati A, Behjati Moghadam M, Ghaderi Segonbad G, Homayouni Tabrizi M (2021) Incorporation of Boswellia sacra essential oil into chitosan/TPP nanoparticles towards improved therapeutic efficiency. Mater Technol 67:1–13
Stella B, Peira E, Dianzani C, Gallarate M, Battaglia L, Gigliotti CL, Boggio E, Dianzani U, Dosio F (2018) Development and characterization of solid lipid nanoparticles loaded with a highly active doxorubicin derivative. Nanomaterials 8(2):110
Tuekaew J, Siriwatanametanon N, Wongkrajang Y, Temsiririrkkul R, Jantan I (2014) Evaluation of the antioxidant activities of Ya-hom Intajak, a Thai herbal formulation, and its component plants. Trop J Pharm Res 13(9):1477–1485
Valeur E, Knerr L, Ölwegård-Halvarsson M, Lemurell M (2017) Targeted delivery for regenerative medicines: an untapped opportunity for drug conjugates. Drug Discovery Today 22(6):841–847
Wang W, Chen T, Xu H, Ren B, Cheng X, Qi R, Liu H, Wang Y, Yan L, Chen S (2018) Curcumin-loaded solid lipid nanoparticles enhanced anticancer efficiency in breast cancer. Molecules 23(7):1578
Ye C, Zhang C, Huang H, Yang B, Xiao G, Kong D, Tian Q, Song Q, Song Y, Tan H (2018) The natural compound myricetin effectively represses the malignant progression of prostate cancer by inhibiting PIM1 and disrupting the PIM1/CXCR4 interaction. Cell Physiol Biochem 48(3):1230–1244

Ying X-Y, Cui D, Yu L, Du Y-Z (2011) Solid lipid nanoparticles modified with chitosan oligosaccharides for the controlled release of doxorubicin. Carbohyd Polym 84(4):1357–1364
Zhang M-J, Su H, Yan J-Y, Li N, Song Z-Y, Wang H-J, Huo L-G, Wang F, Ji W-S, Qu X-J (2018a) Chemopreventive effect of Myricetin, a natural occurring compound, on colonic chronic inflammation and inflammation-driven tumorigenesis in mice. Biomed Pharmacother 97:1131–1137
Zhang Y, Chen X, Gueydan C, Han J (2018b) Plasma membrane changes during programmed cell deaths. Cell Res 28(1):9–21
Zhu W-T, Liu S-Y, Wu L, Xu H-L, Wang J, Ni G-X, Zeng Q-B (2017) Delivery of curcumin by directed self-assembled micelles enhances therapeutic treatment of non-small-cell lung cancer. Int J Nanomed 12:2621

Publisher's Note